High-Performance Sodium Secondary Batteries Using Synergistic Effect of Amorphous SiP/C Anode and Ionic Liquid Electrolyte

AUTHOR(S):

Xinyue, Zhang; Kaushik, Shubham; Matsumoto, Kazuhiko; Hagiwara, Rika

CITATION:

Xinyue, Zhang ...[et al]. High-Performance Sodium Secondary Batteries Using Synergistic Effect of Amorphous SiP/C Anode and Ionic Liquid Electrolyte. Journal of the Electrochemical Society 2020, 167(7): 070514.

ISSUE DATE:

2020-01-05

URL:

http://hdl.handle.net/2433/251474

Journal of The Electrochemical Society, 2020 **167** 070514

High-Performance Sodium Secondary Batteries Using Synergistic Effect of Amorphous SiP_2/C Anode and Ionic Liquid Electrolyte

Zhang Xinyue,[1] Shubham Kaushik,[1,2] Kazuhiko Matsumoto,[1,2,*,z] and Rika Hagiwara[1,2,*]

[1]*Graduate School of Energy Science, Kyoto University, Kyoto 606-8501, Japan*
[2]*Unit of Elements Strategy Initiative for Catalysts & Batteries (ESICB), Kyoto University, Kyoto 615-8510, Japan*

A silicon diphosphide-carbon composite (SiP_2/C) was investigated as a negative electrode material for sodium secondary batteries with the Na[FSA]–[C_3C_1pyrr][FSA] (FSA^- = bis(fluorosulfonyl)amide anion and $C_3C_1pyrr^+$ = *N*-methyl-*N*-propylpyrrolidinium cation) ionic liquid electrolyte. Two amorphous silicon diphosphide materials, SiP_2/C (80:20) and SiP_2/C (70:30) (80:20 and 70:30 refer to the SiP_2:C weight ratio), were prepared by a facile two-step high energy ball-milling process. SiP_2/C (80:20) and SiP_2/C (70:30) delivered high discharge capacities of 883 and 791 mAh g^{-1}, respectively, at 100 mA g^{-1} in the first cycle at 90 °C, with the latter showing better cyclability. Comparison of the performance of SiP_2/C (70:30) in the ionic liquid and organic electrolytes at 25 °C indicated the advantage of the ionic liquid electrolyte in terms of higher discharge capacity and improved cyclability. Electrochemical impedance spectroscopy revealed that the interfacial resistance decreased with cycling in the ionic liquid electrolyte at 25 °C but significantly increased at 90 °C. Ex situ X-ray diffraction revealed that the product remains amorphous even after charging and discharging in SiP_2/C (70:30). This study demonstrated the importance of ionic liquids and phosphide based materials as high performance enablers for sodium secondary batteries.
 [DOI: 10.1149/1945-7111/ab69f8]

Manuscript submitted October 22, 2019; revised manuscript received January 2, 2020. Published January 23, 2020. *This paper is part of the JES Focus Issue on Challenges in Novel Electrolytes, Organic Materials, and Innovative Chemistries for Batteries in Honor of Michel Armand.*

Supplementary material for this article is available online

In the recent decades, lithium-ion batteries (LIBs) have been widely accepted as a primary energy storage system in daily life because of their high energy density and low degree of self-discharge.[1–3] However, owing to the limited and uneven distribution of lithium and cobalt resources,[4,5] the search for new energy storage technologies is inevitable, especially for large-scale applications.[6,7] Sodium, which belongs to the same group as lithium in the periodic table and has the second smallest size, has similar properties as lithium besides having a low standard electrode potential (−2.71 V vs standard hydrogen electrode); furthermore, sodium resources are evenly distributed in the Earth's crust and seawater.[8] Therefore, sodium secondary batteries can be considered as alternatives to LIBs, especially for large-scale energy storage systems.[9–16] Although the properties of sodium and lithium are similar, the technology transfer from LIBs to sodium secondary batteries is not always straightforward; a typical example of such a case is the difficulty in the intercalation of sodium ions into graphite.[17] Thus, the facile preparation of a suitable negative electrode material that has high reversible capacity, high rate capability, and long lifespan is one of the key challenges in the development of sodium secondary batteries.[18,19]

Currently, insertion materials,[20–27] conversion materials,[28–34] and alloy materials[35–41] are investigated for use as negative electrode materials in sodium secondary batteries. Among alloy materials, elemental phosphorus has attracted much attention due to its large theoretical capacity (~2596 mAh g^{-1}) and moderate operating voltage.[42] However, the extremely low electronic conductivity of red phosphorus (10^{-14} s cm^{-1}) and the stress caused by the volume expansion after sodiation, which is accompanied by pulverization, result in a short cycle life.[43] The use of binary phosphides such as Sn_4P_3,[44] GeP_5/C,[45] FeP_4,[46] and CuP_2/C[47] has been reported to alleviate the aforementioned problem by providing electronic conduction pathways and buffering the large volume change. Nevertheless, the limited abundance of metals such as tin and the moderate cyclability motivates researchers to investigate other binary phosphides.

Recently, SiP_2 has emerged as a desirable candidate for a negative electrode in sodium secondary batteries, as it consists of abundant elements and exhibits a high theoretical capacity of 1780 mAh g^{-1}, assuming Si and Na_3P are completely charged species. A previous study on SiP_2 revealed a high discharge capacity of 843 mA h g^{-1} in the first cycle, but rapid capacity fading occurred in the subsequent cycles.[48] Better cyclability was achieved by ball-milling SiP_2 with carbon black[49] and multiwalled carbon nanotubes (MWCNT).[50] However, the introduction of a large amount of carbon materials increases the specific surface area, thus accelerating electrolyte decomposition during the first charging step and a low initial Coulombic efficiency. Amorphization of compounds sometimes improves the capacity owing to the formation of random reaction pathways.[51,52] Crystalline silicon is known to be inactive for sodiation, but amorphous silicon has demonstrated a capacity of 80 mAh g^{-1}.[53] Hence, amorphous SiP_2 carbon composite is a potential negative electrode to achieve high electrochemical performance for sodium secondary batteries.

Appropriate choice of the electrolyte is crucial to obtain high performance, long cycle life, and safety in secondary batteries.[12,54–56] Ionic liquids (ILs) have been widely developed and applied in batteries due to their advantages of extremely low vapor pressure, high thermal stability, low melting point, and wide electrochemical window compared with traditional organic solvents.[57–59] Some studies showed the superior performance in IL than organic electrolytes.[60,61] A full cell fabricated with $Na_{0.44}MnO_2$ with hard carbon demonstrated better cyclability and lower charge transfer resistance in Na[FSA]-[C_3C_1pyrr][FSA] than the conventional $NaClO_4$ in EC/DEC organic electrolyte.[62] Moreover, some composite materials like Sb_2S_3/graphene[63] and SnO_2/graphene[64] exhibited improved rate and cyclability using ILs than organic electrolytes at both 25 °C and 60 °C. The role of the IL electrolyte in the formation of a robust and stable solid electrolyte interface (SEI) film is also an important factor to be considered in improving the long-term cycle stability of the battery,[65–69] which is manifested in the conversion based negative electrode with the serious problem of volume expansion.[70,71] Moreover, intermediate temperature operation with ILs, achieved by

*Electrochemical Society Member.
[z]E-mail: k-matsumoto@energy.kyoto-u.ac.jp

the economical use of waste heat, greatly improves the ion transport and interfacial reactions, which is highly desirable in high-power-density applications.[72–74] Recently, a diverse range of ILs have been explored as electrolytes for sodium secondary batteries[75–77]; in particular, the Na[FSA]–[C_3C_1pyrr][FSA] IL exhibits high performance for this purpose.[78,79] It has been demonstrated that Na[FSA]–[C_3C_1pyrr][FSA] (2:8 molar ratio, IL_{FSA}) has electrochemical window of 5.2 V and ionic conductivity of 19.8 mS cm^{-1} at 90 °C and exhibits stable Na metal deposition/dissolution.[80,81] This electrolyte also derives high cyclability and rate performance of phosphorus-based compounds (Sn_3P_4,[28] CuP_2/C,[82] $V_4P_7/5P$[83]) owing to the robust SEI layer formation, low interfacial resistance, and high ionic conductivity. The Na salt concentration around 1 M for this IL electrolyte also makes comparison of electrochemical data with other cases easier. In this work, the phosphide chemistry in an IL electrolyte is extended to SiP_2, and the electrochemical behavior of the SiP_2/C negative electrode in the IL_{FSA} is investigated at 25 °C and 90 °C.

Experimental

Material preparation.—The silicon phosphide (SiP_2) sample was prepared by high-energy ball-milling (HEBM) of Si (Kojundo Chemical Laboratory, purity 99.9%) and phosphorus powder (Wako Pure Chemical Industries, purity 98%) in a stoichiometric ratio (1:2 in mol) under Ar atmosphere with a ball to powder weight ratio of 35:1. The ball-milling process was carried out at 800 RPM for 5, 10, and 20 h to optimize the reaction time for the formation of SiP_2. The resulting powder was collected from the vessel and ball-milled again with either 20% or 30% weight ratio of acetylene black (AB; Wako Pure Chemical Industries) separately under the same conditions for 3 h to obtain the SiP_2/C composite. The effect of ball-milling time on crystallinity was also investigated.

Characterization.—The X-ray diffraction (XRD) patterns of the samples were obtained on a Rigaku SmartLab diffractometer (CuKα (1.5418 Å), 40 kV–30 mA) under Ar atmosphere. The samples were sealed in an airtight cell with Be windows under an Ar atmosphere and set on the diffractometer. The XRD patterns were recorded in the 2θ range of 20–70°. X-ray photoelectron spectroscopy (XPS) measurements were carried out using a JEOL JPS-9010 spectrometer (MgKα, 10 kV–10 mA). The spectra were calibrated by using C1s (284.5 eV) as a reference. The particle size and morphology were determined by scanning electron microscopy (SEM; Hitachi SU-8020), and elemental mapping analysis was performed by energy-dispersive X-ray spectroscopy (EDX; Horiba EMAX Evolution X-max), respectively.

Cell fabrication and electrochemical characterization.—The negative electrode was prepared by mixing the active material (SiP_2/C), AB, and polyamide-imide binder (75:15:10 by weight) in *N*-methyl-2-pyrrolidone (NMP; Wako Pure Chemical Industries, purity 99%) using a planetary centrifugal mixer (AR-100, Thinky). The resulting slurry was cast on Al foil (20 μm) and dried under vacuum at 90 °C for 10 h in an oven and on a vacuum line at 110 °C for 48 h. The loading mass of active material was in the range of 0.75–1 mg cm^2. IL_{FSA} was prepared by mixing the two pre-dried salts (Na[FSA], Mitsubishi Materials Electronic Chemicals Co., Ltd, purity >99%; [C_3C_1pyrr][FSA], Kanto Chemical Co., Inc., purity >99.9%), in a 2:8 molar ratio and further vacuum-dried at 90 °C for 24 h. An organic electrolyte of 1 M Na[FSA] in ethylene carbonate/dimethyl carbonate (1:1 v/v) (ORG_{FSA}) was also used for comparison. A glass fiber filter (Whatman, GFA, 260 mm in thickness and 16 mm in diameter) was used as a separator. A sodium metal disc (Aldrich, purity 99.9%) was used as the counter electrode. The coin cell (2032-type) was assembled in a glove box filled with Ar (O_2 < 1 ppm, dew point: <−90 °C) for measuring the electrochemical performance.

Electrochemical performance was measured using a HJ1001SD8 charge-discharge test device (Hokuto Denko). All the coin cells were held at the open-circuit voltage for least 3 h in an ESPEC thermostatic chamber before the measurements.

For ex situ XRD measurements, the electrodes were charged and discharged to the desired voltage, recovered by disassembling the coin cell, rinsed with tetrahydrofuran, and dried under vacuum for several hours prior to the measurements. Electrochemical impedance spectroscopy (EIS) was performed on a VSP potentiostat (Bio-Logic) at 25 °C and 90 °C over the frequency range from 100 mHz to 100 kHz, with an AC amplitude of 20 mV. The symmetric cells were prepared using 2032 coin cells by replacing sodium metal with SiP_2/C in normal half-cell configurations. EIS profiles were obtained at 0.5 V in the charging step of the (n + 1)th cycle (n = 1, 3, 10, 50).

Results and Discussion

Three reaction times (5, 10, and 20 h) for ball-milling silicon with phosphorus were tested to prepare SiP_2, and a ball-milling time of 20 h was found to be necessary to complete the reaction (Fig. S1, supplementary information is available online at stacks.iop.org/JES/167/070514/mmedia). The SiP_2 peaks appeared after 10 h of ball-milling, and the Si peaks completely disappeared after 20 h. The following experiments were conducted for the SiP_2 sample with 20 h of ball-milling. The resulting SiP_2 was further ball-milled with conductive carbon in SiP_2:C ratios of 80:20 and 70:30 (SiP_2/C (80:20) and SiP_2/C (70:30)) to enhance the electronic conductivity. The XRD patterns of the as-prepared SiP_2, SiP_2/C (80:20) and SiP_2/C (70:30) are shown in Figs. 1a–1c, respectively. All the diffraction peaks of SiP_2 were indexed to the pyrite-type SiP_2 phase.[84] However, after ball-milling with AB, all the SiP_2 peaks disappeared in the spectra of both the SiP_2/C (80:20) and SiP_2/C (70:30) powders, indicating amorphization of the material. This phenomenon is commonly observed[85–87] during ball-milling under intense conditions due to the continuous heavy impact and abrasion of the particles.

Figure 2 shows the XPS profiles of (a) SiP_2/C (80:20) and (b) SiP_2/C (70:30) in the P 2p region. The peak around 129 eV in both cases confirms the formation of SiP_2 respectively. However, the peaks showed a slight shift to the lower-energy side as compared to the literature data,[88] which could be due to ball-milling at a very high speed. The peak at 132.5 eV, corresponding to the P-O-C bond, was significantly more intense than the SiP_2 peak, indicating that the majority of the phosphorus on the particle surface is present in this form. A recent report on a ball-milled SiP_2/CNT composite also confirmed the formation of a P-O-C bond.[89] This P-O-C bond is responsible for good cyclability as it restricts volume change and

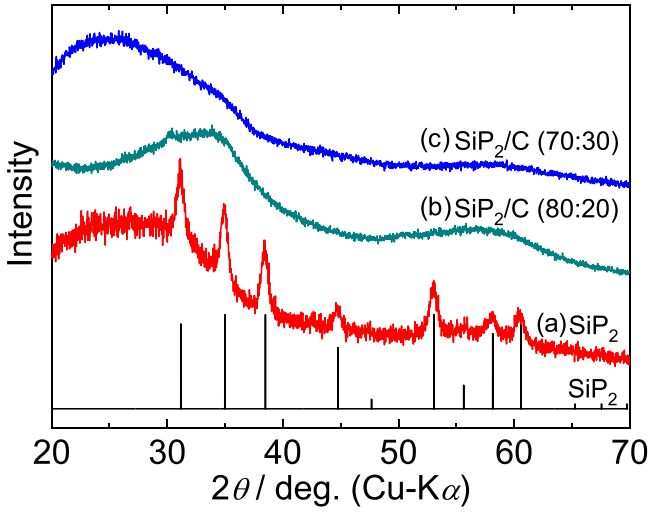

Figure 1. XRD patterns of (a) as-prepared SiP_2, (b) SiP_2/C (80:20), and (c) SiP_2/C (70:30). The reference pattern of pyrite-type SiP_2[84] is shown for comparison.

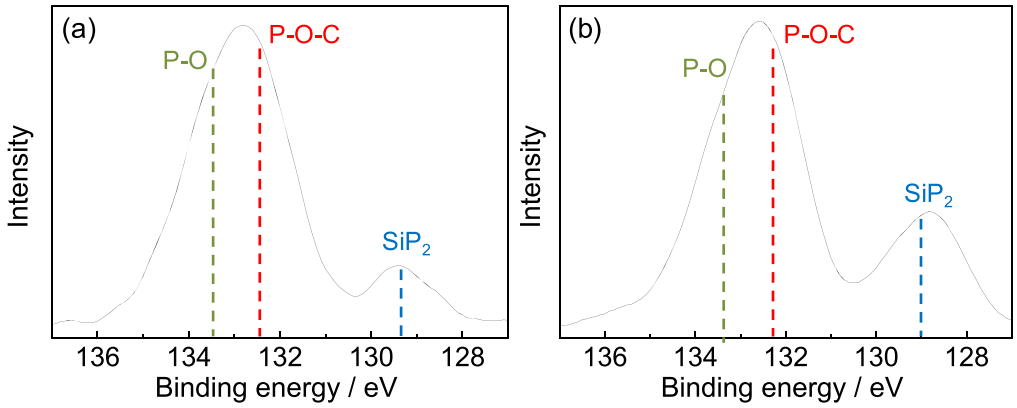

Figure 2. XPS (P 2p) profiles of (a) SiP_2/C (80:20) and (b) SiP_2/C (70:30).

provides high electrical conductivity, which preserves interparticle connectivity even after long-term cycling.[90–92]

Figure S2 shows the SEM images and EDX maps of the (a, b) SiP_2, (c, d) SiP_2/C (80:20) and (e, f) SiP_2/C (70:30) composites, revealing the morphological characteristics as irregular aggregates of 50–500 nm in size and uniform distribution of elements.

The galvanostatic charge/discharge profiles of the as-prepared SiP_2, SiP_2/C (80:20), and SiP_2/C (70:30) in IL_{FSA} at 90 °C are shown in Figs. 3a–3c, respectively (current density: 100 mA g^{-1} and voltage range: 0.005−2.0 V). SiP_2 without conductive carbon delivered a large initial charge capacity of 1153 mAh g^{-1} (Fig. 3a), but the discharge capacity was merely 226 mAh g^{-1}, giving a Coulombic efficiency of 20%. This result could be attributed to the difficulty in sodium extraction because of the low electrical conductivity of SiP_2. On the other hand, SiP_2/C (80:20) and SiP_2/C (70:30) demonstrated high reversible discharge capacities of 883 and 791 mAh g^{-1} with Coulombic efficiencies of 72% and 76% in the first cycle (Figs. 3b and 3c), respectively. The irreversible capacity was partially due to the reductive decomposition of the electrolyte on the electrode surface to form the SEI layer. The drastic increase in the first cycle Coulombic efficiency as compared to that of the as-prepared SiP_2 suggests the important role of the conductive carbon. The charge-discharge curves of the subsequent cycles essentially overlapped with each other, indicating good reversibility of the sodiation and desodiation processes in the SiP_2/C composite at 90 °C. The redox activity of SiP_2 and SiP_2/C (70:30) against voltage was quantified by dQ/dV plots as shown in Fig. S3. During the first cathodic scan of the SiP_2 electrode (Fig. S3a), the two peaks in the range between 1.0 and 1.5 V can be attributed to electrolyte decomposition because of the irreversibility of the peaks, and the following large peak starting at 0.13 V corresponds to sodiation of SiP_2. During the anodic process, a three step desodiation process was observed around 0.1, 0.25, and 0.8 V. In the second and third cycle, limited redox activities were observed during the cathodic process detected only in the low voltage zone. The weakened peak intensity and shifting to higher voltage during

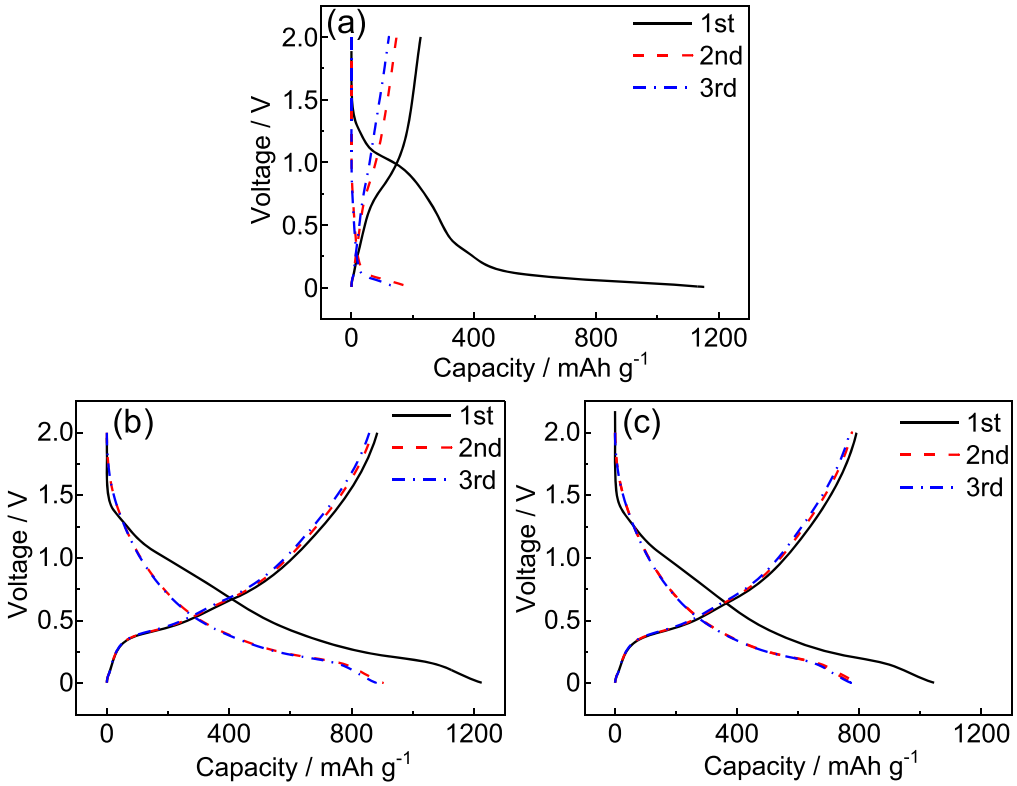

Figure 3. Galvanostatic charge-discharge curves of (a) as-prepared SiP_2, (b) SiP_2/C (80:20), and (c) SiP_2/C (70:30) electrodes in IL_{FSA} at 90 °C (rate: 100 mA g^{-1}, voltage range: 0.005–2.000 V).

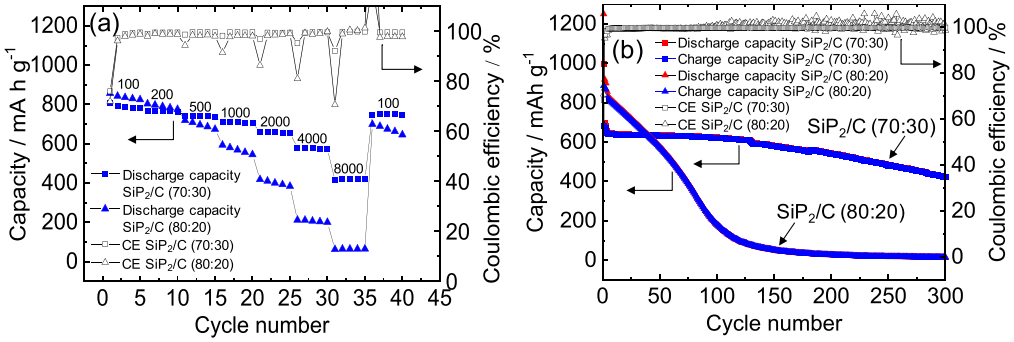

Figure 4. (a) Rate capability of SiP_2/C (80:20) and SiP_2/C (70:30) electrodes at 90 °C (rate: 100–8000 mAg^{-1}) and (b) cyclability at 90 °C (rate: 500 mAg^{-1}, first three cycles at 100 mAg^{-1}).

the anodic process shows increasing polarization with cycling. On the other hand, better reversibility was observed in SiP_2/C (70:30) case. In the first cycle, two small peaks corresponding to the electrolyte decomposition around 1.3 and 1.0 V and one sodiation peak at 0.2 V were observed during the cathodic process (Fig. S3 b). Subsequently, the desodaition took place with three steps at 0.1, 0.4 and 0.65 V. The sodiation and desodiation was reversible in the second and third cycles, indicating the important role of AB to maintain the redox activity.

Figure 4 represents the rate capability and cyclability of SiP_2/C (80:20) and SiP_2/C (70:30) with IL_{FSA} at 90 °C. The SiP_2/C (70:30) showed superior rate performance to that of SiP_2/C (80:20), with a discharge capacity of 790 mAh g^{-1} at 100 mA g^{-1}, 740 mAh g^{-1} at 500 mA g^{-1}, 710 mAh g^{-1} at 1000 mA g^{-1}, and 420 mAh g^{-1} at 8000 mA g^{-1}, as shown in Fig. 4a. Figure 4b shows the cycling performance of SiP_2/C (80:20) and SiP_2/C (70:30) at 500 mAg^{-1}, after electrochemical activation for the first three cycles at 100 mA g^{-1}. The SiP_2/C (70:30) composite exhibited stable cycling with more than 65% capacity retention after 300 cycles, with a Coulombic efficiency of 99.7%. Although high capacity was observed for SiP_2/C (80:20) during the initial cycles, severe capacity degradation was observed in the first 100 cycles with a large fluctuation in the Coulombic efficiency. The superior performance of SiP_2/C (70:30) over that of SiP_2/C (80:20) was attributed to the restriction of pulverization owing to the presence of a P-O-C bond and the high electronic conductivity with the 30% conductive carbon in the composite. Therefore, further investigations were carried out only on SiP_2/C (70:30) as described below.

The electrochemical performance of SiP_2/C (70:30) at 25 °C was compared between the Na[FSA]-based organic electrolyte, ORG_{FSA} (see Experimental section for details on this electrolyte) and IL_{FSA} (~1 M). Figures 5a and 5b show the charge–discharge curves of SiP_2/C (70:30) in ORG_{FSA} and IL_{FSA}, respectively, for the initial 5 cycles. Although the charge capacity with ORG_{FSA} in the first cycle was similar to that of IL_{FSA}, the discharge capacities in the second cycle were significantly different from each other (400 mAh g^{-1} in ORG_{FSA} and 600 mAh g^{-1} in IL_{FSA}), indicating the different functionality of the two electrolytes. This observation agrees with those in previous reports; IL_{FSA} was reported to provide a uniform and robust SEI layer with electrode materials such as elemental phosphorus and metal phosphides.[28,71] According to previous work,[49] better performance of SiP_2/C (60:40) was obtained with an organic electrolyte. The different behavior is considered to arise from the larger carbon content and the use of a fluoroethylene carbonate additive. Other electrochemical tests with IL_{FSA} also showed considerably superior performance of SiP_2/C (70:30) at

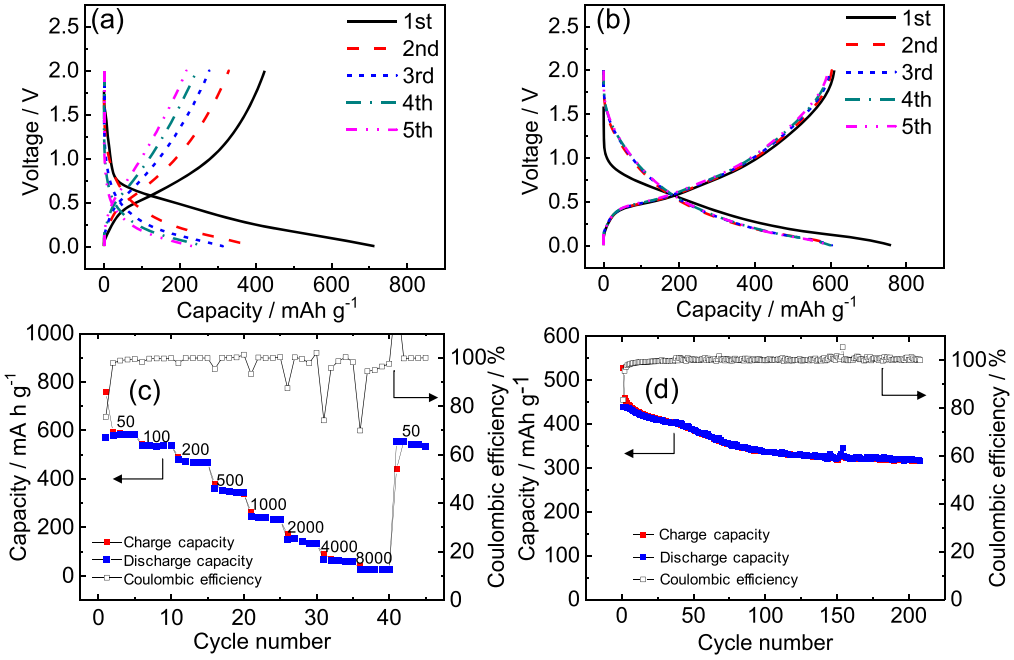

Figure 5. Galvanostatic charge-discharge curves of SiP_2/C (70:30) at 25 °C with (a) ORG_{FSA} and (b) IL_{FSA} (rate: 100 mA g^{-1}, voltage range: 0.005–2.000 V). (c) rate capability test (rate: 100–8000 mA g^{-1}) with IL_{FSA}, and (d) cyclability (rate: 200 mAg^{-1}, initial three cycles at 100 mA g^{-1}) with IL_{FSA}. The Coulombic efficiency in the 41st cycle in (c) is 126.7%.

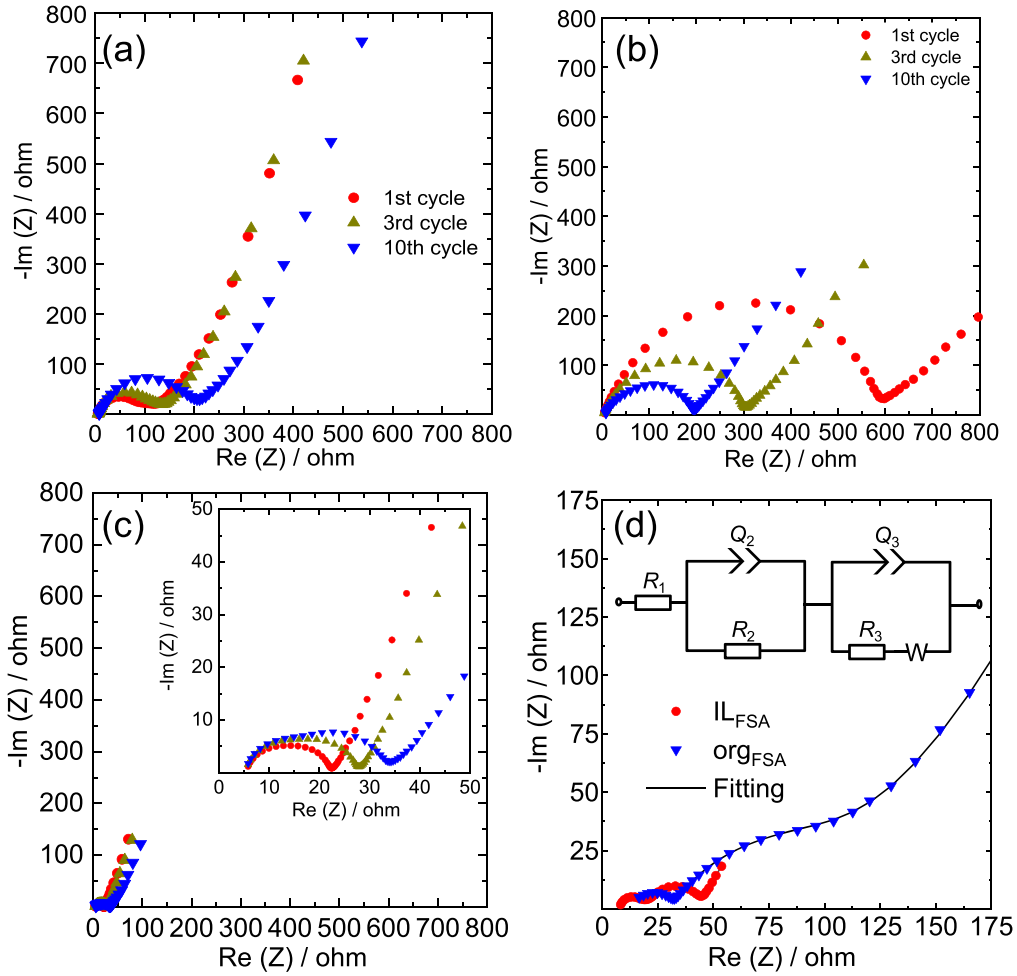

Figure 6. Results of EIS tests for the SiP_2/C (70:30) electrode. (a)–(c) Nyquist plots of the Na||SiP_2/C cell with cycling at (a) 25 °C with ORG_{FSA}, (b) 25 °C with IL_{FSA}, and (c) 90 °C with IL_{FSA} (inset magnified view). (d) Nyquist plots of SiP_2/C||SiP_2/C symmetric cell at 25 °C with ORG_{FSA} and IL_{FSA}. For (a)–(c), galvanostatic charge-discharge was performed in the half-cell at a rate of 100 mA g^{-1} in the first 10 cycles and 500 mA g^{-1} in 11–50 cycles. EIS measurements were performed at 0.5 V during charging, in the $n + 1$ cycle (n = 1, 3, 10, 50). For the symmetric cell impedance in (d), the electrodes were charged and discharged for 1 cycle and charged again to 0.5 V in half cells and disassembled for preparation of the symmetric cells.

25 °C. In the rate test, capacities of 540, 340, 240, and 30 mAh g^{-1} were obtained at 100, 500, 1000, and 8000 mA g^{-1}, respectively (Fig. 5c). SiP_2/C (70:30) also exhibited high cyclability at the rate of 500 mA g^{-1} over 200 cycles (Fig. 5d), as characterized by the 73% capacity retention. The aforementioned results suggest that the SiP_2/C (70:30) is suitable for use as a high-performance negative electrode with long term cyclability and high-rate applications at both 25 and 90 °C.

To elucidate the difference in cyclability observed in IL and organic electrolytes, EIS measurements were performed on a Na||SiP_2/C half-cell with cycling and a symmetric cell SiP_2/C||SiP_2/C after one cycle using IL_{FSA} and ORG_{FSA}. The EIS results were compared for the SiP_2/C(70:30) electrode charged to 0.5 V. Figures 6a and 6b show the Nyquist plots for the Na||SiP_2/C half-cell during cycling at 25 °C with IL_{FSA} and ORG_{FSA}, respectively. With progressive cycling, the interfacial resistance for IL_{FSA} considerably decreased, whereas that for ORG_{FSA} increased. Figure 6c shows the Nyquist plots for Na||SiP_2/C with IL_{FSA} during cycling at 90 °C. The interfacial resistance reduced significantly at 90 °C as compared to that at 25 °C, because of the low interfacial resistance offered by sodium metal at 90 °C.[65] The high rate capability obtained at 90 °C could be explained by this result. Figure 6d shows the Nyquist plots of the SiP_2/C||SiP_2/C symmetric cell after 1 cycle at 25 °C with the IL_{FSA} and ORG_{FSA} electrolytes. The use of a symmetric cell is preferable to exclude the effects of the sodium metal counter electrode. Two semicircles were observed in both cases, with a sloping curve denoting the diffusion behavior. The EIS curves were well-fitted by the corresponding parameters according to the equivalent circuit in the inset of Fig. 6d (see Table SI and Table SII for the optimized parameters for symmetric cell and half-cell, respectively). The R_2 value was similar in both the cases, but R_3 was considerably higher for the organic electrolyte. The characteristic frequencies accompanying R_2 and R_3 decreased in the high- and low-frequency regions, respectively. The resistances at high and low frequencies are generally related to the surface film layer resistance and charge transfer resistance, respectively.[65] Thus, it can be suggested that the increase in charge transfer resistance after cycling may be the reason behind the poor cyclability in the organic electrolyte.

The mechanism underlying the electrochemical reactions for SiP_2/C (70:30) in IL_{FSA} at 90 °C was investigated by ex situ XRD analysis (Fig. 7). The SiP_2/C (70:30) electrode is amorphous before the reactions, as shown in Fig. 1b, but some unknown peaks were observed at 23.9° and 46.7° in the pristine electrode, which may arise from the impurity introduced during the electrode washing or XRD measurements. After charging and discharging, no new peak appeared in the XRD patterns, indicating that all the products are amorphous. This reaction mechanism is different from the previously reported one, which suggested the formation of Na_3P and $NaSi_6$ during the charging process and re-formation of amorphous SiP_2 and phosphorus during the discharge process.[49] Differences in the crystallinity of the electrode material, reaction temperature, and

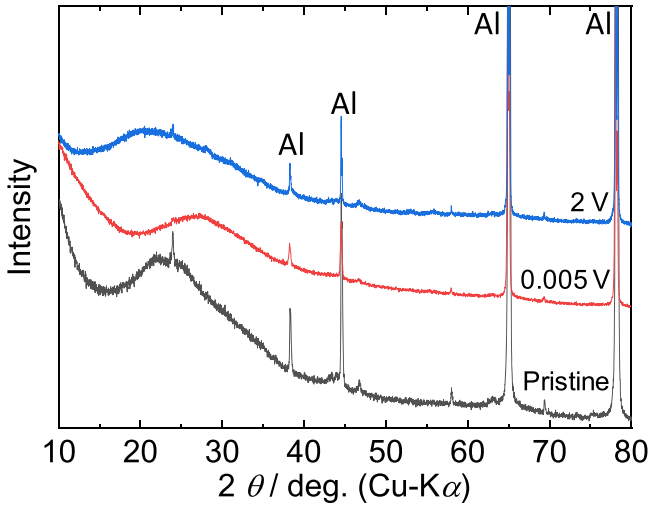

Figure 7. Ex situ XRD patterns of SiP_2/C (70:30) electrode (pristine, charging: 0.005 V, and discharging: 2 V) during the first cycle. Electrolyte: IL_{FSA}. Temperature of charge-discharge: 90 °C. The small peaks at 58.1° and 69.2° are identified as the aluminum Kβ peaks at 65.0° and 78.3°.

electrolyte possibly cause such differences. The large capacity attained at 90 °C led to a deeper charging state and affected the reaction mechanism (e.g. 790 mAh g^{-1} at 100 mA g^{-1}).

Conclusions

SiP_2, SiP_2/C (80:20), and SiP_2/C (70:30) were prepared by high-energy ball-milling and investigated for use as negative electrodes in sodium secondary batteries. SiP_2/C (70:30) demonstrated better performance than did SiP_2/C (80:20), with high capacity of 420 mAh g^{-1} at a high rate of 8000 mA g^{-1} and 65% capacity retention after 300 cycles at 90 °C in IL_{FSA}. The charge-discharge curves of SiP_2/C (70:30) at 25 °C showed stable cyclability and higher discharge capacity in the case of IL_{FSA} than in the case of ORG_{FSA}. The presence of P-O-C bond, enhanced ionic conductivity of IL and the low interfacial resistance with cycling are suggested to be the reasons for the good performance observed in IL_{FSA}. Symmetric cell EIS measurements on SiP_2/C||IL_{FSA}||SiP_2/C at 25 °C revealed significantly lower charge transfer resistance than that of SiP_2/C||ORG_{FSA}||SiP_2/C after one cycle. The products after charging and discharging were found to be amorphous for SiP_2/C (70:30), in contrast to a previous study where crystalline Na_3P and $NaSi_6$ were observed after first charging. This difference might occur due to differences in the crystallinity of the starting active material and electrolyte as well as the higher depth of charge. The detailed study of charge discharge mechanism is a matter of future investigation. In this report, the obtained results clearly states that the utilization of ionic liquid is beneficial for sodium secondary batteries enabling high performance of SiP_2/C (70:30) and promoting safer operations.

Acknowledgments

This study was supported by the Japanese Ministry of Education, Culture, Sports, Science and Technology (MEXT) program "Elements Strategy Initiative to Form Core Research Center."

References

1. B. Dunn, H. Kamath, and J.-M. Tarascon, *Science*, **334**, 928 (2011).
2. B. Scrosati and J. Garche, *J. Power Sources*, **195**, 2419 (2010).
3. J. B. Goodenough and K.-S. Park, *J. Am. Chem. Soc.*, **135**, 1167 (2013).
4. J.-M. Tarascon, *Nat. Chem.*, **2**, 510 (2010).
5. H. Vikström, S. Davidsson, and M. Höök, *Appl. Energy*, **110**, 252 (2013).
6. A. N. Arnette, *Renew. Sust. Energ. Rev.*, **70**, 254 (2017).
7. G. L. Soloveichik, *Annu. Rev. Chem. Biomol. Eng.*, **2**, 503 (2011).
8. Y. Nozaki, *EOS. Trans*, **78**, 221 (1997).
9. A. Ponrouch, E. Marchante, M. Courty, J.-M. Tarascon, and M. R. Palacín, *Energy Environ. Sci.*, **5**, 8572 (2012).
10. D. Larcher and J. M. Tarascon, *Nat. Chem.*, **7**, 19 (2014).
11. M. S. Islam and C. A. J. Fisher, *Chem. Soc. Rev.*, **43**, 185 (2014).
12. A. Ponrouch, D. Monti, A. Boschin, B. Steen, P. Johansson, and M. R. Palacín, *J. Mater. Chem. A*, **3**, 22 (2015).
13. A. Ponrouch, R. Dedryvère, D. Monti, A. E. Demet, J. M. Ateba Mba, L. Croguennec, C. Masquelier, P. Johansson, and M. R. Palacín, *Energy Environ. Sci.*, **6**, 2361 (2013).
14. K. Kubota and S. Komaba, *J. Electrochem. Soc.*, **162**, A2538 (2015).
15. G. G. Eshetu, S. Grugeon, H. Kim, S. Jeong, L. Wu, G. Gachot, S. Laruelle, M. Armand, and S. Passerini, *ChemSusChem*, **9**, 462 (2016).
16. M. D. Slater, D. Kim, E. Lee, and C. S. Johnson, *Adv. Funct. Mater.*, **23**, 947 (2013).
17. P. Ge and M. Fouletier, *Solid State Ion.*, **28–30**, 1172 (1988).
18. R. Yamamoto, N. Yabuuchi, and M. Miyasaka, *J. Electrochem. Soc.*, **165**, A434 (2018).
19. J. R. González, R. Alcántara, F. Nacimiento, G. F. Ortiz, and J. L. Tirado, *J. Electrochem. Soc.*, **162**, A3007 (2014).
20. C. Ding, T. Nohira, and R. Hagiwara, *J. Mater. Chem. A*, **3**, 20767 (2015).
21. H. Usui, S. Yoshioka, K. Wasada, M. Shimizu, and H. Sakaguchi, *ACS Appl. Mater. Interfaces*, **7**, 6567 (2015).
22. A. Rudola, K. Saravanan, C. W. Mason, and P. Balaya, *J. Mater. Chem. A*, **1**, 2653 (2013).
23. P. Senguttuvan, G. Rousse, V. Seznec, J.-M. Tarascon, and M. R. Palacín, *Chem. Mater.*, **23**, 4109 (2011).
24. B. Zhang, R. Dugas, G. Rousse, P. Rozier, A. M. Abakumov, and J.-M. Tarascon, *Nat. Commun.*, **7**, 10308 (2016).
25. A. Eguía-Barrio, E. Castillo-Martínez, M. Zarrabeitia, M. A. Muñoz-Márquez, M. Casas-Cabanas, and T. Rojo, *Phys. Chem. Chem. Phys.*, **17**, 6988 (2015).
26. M. M. Doeff, Y. Ma, S. J. Visco, and L. C. De Jonghe, *J. Electrochem. Soc.*, **140**, L169 (1993).
27. E. Irisarri, A. Ponrouch, and M. R. Palacin, *J. Electrochem. Soc.*, **162**, A2476 (2015).
28. H. Usui, Y. Domi, K. Fujiwara, M. Shimizu, T. Yamamoto, T. Nohira, R. Hagiwara, and H. Sakaguchi, *ACS Energy Lett.*, **2**, 1139 (2017).
29. F. Klein, B. Jache, A. Bhide, and P. Adelhelm, *Phys. Chem. Chem. Phys.*, **15**, 15876 (2013).
30. I. Hasa, R. Verrelli, and J. Hassoun, *Electrochim. Acta*, **173**, 613 (2015).
31. G. Longoni, M. Fiore, J.-H. Kim, Y. H. Jung, D. K. Kim, C. M. Mari, and R. Ruffo, *J. Power Sources*, **332**, 42 (2016).
32. Z. Huang, H. Hou, C. Wang, S. Li, Y. Zhang, and X. Ji, *Chem. Mater.*, **29**, 7313 (2017).
33. G.-Y. Chen, Q. Sun, J.-L. Yue, Z. Shadike, Y. Yang, F. Ding, L. Sang, and Z.-W. Fu, *J. Power Sources*, **284**, 115 (2015).
34. H. Tao, M. Zhou, R. Wang, K. Wang, S. Cheng, and K. Jiang, *Adv. Sci.*, **5**, 1801021 (2018).
35. T. Yamamoto, T. Nohira, R. Hagiwara, A. Fukunaga, S. Sakai, K. Nitta, and S. Inazawa, *Electrochim. Acta*, **135**, 60 (2014).
36. H. Xie, W. P. Kalisvaart, B. C. Olsen, E. J. Luber, D. Mitlin, and J. M. Buriak, *J. Mater. Chem. A*, **5**, 9661 (2017).
37. M. Hu, Y. Jiang, W. Sun, H. Wang, C. Jin, and M. Yan, *ACS Appl. Mater. Interfaces*, **6**, 19449 (2014).
38. L. Wu, H. Lu, L. Xiao, J. Qian, X. Ai, H. Yang, and Y. Cao, *J. Mater. Chem. A*, **2**, 16424 (2014).
39. M. Lao, Y. Zhang, W. Luo, Q. Yan, W. Sun, and S. X. Dou, *Adv. Mater.*, **29**, 1700622 (2017).
40. Y. Zhao and A. Manthiram, *Chem. Mater.*, **27**, 3096 (2015).
41. H. Tan, D. Chen, X. Rui, and Y. Yu, *Adv. Funct. Mater.*, **29**, 1808745 (2019).
42. J. Qian, X. Wu, Y. Cao, X. Ai, and H. Yang, *Angew. Chem. Int. Ed.*, **52**, 4633 (2013).
43. Y. Kim, Y. Park, A. Choi, N.-S. Choi, J. Kim, J. Lee, J. H. Ryu, S. M. Oh, and K. T. Lee, *Adv. Mater.*, **25**, 3045 (2013).
44. H. Usui, Y. Domi, H. Nishida, K. Yamaguchi, R. Yamagami, and H. Sakaguchi, *ChemistrySelect*, **3**, 8462 (2018).
45. W. Li, L. Ke, Y. Wei, S. Guo, L. Gan, H. Li, T. Zhai, and H. Zhou, *J. Mater. Chem. A*, **5**, 4413 (2017).
46. W. Zhang, M. Dahbi, S. Amagasa, Y. Yamada, and S. Komaba, *Electrochem. Commun.*, **69**, 11 (2016).
47. S.-O. Kim and A. Manthiram, *Chem. Commun.*, **52**, 4337 (2016).
48. D. Duveau, S. S. Israel, J. Fullenwarth, F. Cunin, and L. Monconduit, *J. Mater. Chem. A*, **4**, 3228 (2016).
49. J. Saddique et al., *ACS Appl. Energy Mater.*, **2**, 2223 (2019).
50. C.-Y. Wang, Y.-H. Yi, W.-C. Chang, T.-L. Kao, and H.-Y. Tuan, *J. Power Sources*, **399**, 49 (2018).
51. Y. Nagata, K. Nagao, M. Deguchi, A. Sakuda, A. Hayashi, H. Tsukasaki, S. Mori, and M. Tatsumisago, *Chem. Mater.*, **30**, 6998 (2018).
52. J. Ye, P. Shea, A. C. Baumgaertel, S. A. Bonev, M. M. Biener, M. Bagge-Hansen, Y. M. Wang, J. Biener, and B. C. Wood, *Chem. Mater.*, **30**, 8871 (2018).
53. C.-H. Lim, T.-Y. Huang, P.-S. Shao, J.-H. Chien, Y.-T. Weng, H.-F. Huang, B. J. Hwang, and N.-L. Wu, *Electrochim. Acta*, **211**, 265 (2016).
54. K. Xu, *Chem. Rev.*, **114**, 11503 (2014).
55. Y.-M. Lin, K. C. Klavetter, P. R. Abel, N. C. Davy, J. L. Snider, A. Heller, and C. B. Mullins, *Chem. Commun.*, **48**, 7268 (2012).
56. J. Y. Jang, H. Kim, Y. Lee, K. T. Lee, K. Kang, and N.-S. Choi, *Electrochem. Commun.*, **44**, 74 (2014).
57. M. Armand, F. Endres, D. R. MacFarlane, H. Ohno, and B. Scrosati, *Nat. Mater.*, **8**, 621 (2009).

58. H. Ohno, in *Electrochemical Aspects of Ionic Liquids* (John Wiley & Sons Inc., Hoboken, NJ) (2011).
59. M. Watanabe, M. L. Thomas, S. Zhang, K. Ueno, T. Yasuda, and K. Dokko, *Chem. Rev.*, **117**, 7190 (2017).
60. K. Matsumoto, J. Hwang, S. Kaushik, C.-Y. Chen, and R. Hagiwara, *Energy Environ. Sci.*, **12**, 3247 (2019).
61. A. K. Tripathi and R. K. Singh, *J. Energy Storage*, **15**, 283 (2018).
62. C.-H. Wang, C.-H. Yang, and J.-K. Chang, *Chem. Commun.*, **52**, 10890 (2016).
63. C.-Y. Li, J. Patra, C.-H. Yang, C.-M. Tseng, S. B. Majumder, Q.-F. Dong, and J.-K. Chang, *ACS Sustain. Chem. Eng.*, **5**, 8269 (2017).
64. H.-C. Chen, J. Patra, S.-W. Lee, C.-J. Tseng, T.-Y. Wu, M.-H. Lin, and J.-K. Chang, *J. Mater. Chem. A*, **5**, 13776 (2017).
65. J. Hwang, K. Matsumoto, and R. Hagiwara, *J. Phys. Chem. C*, **122**, 26857 (2018).
66. J. Zheng, M. Gu, H. Chen, P. Meduri, M. H. Engelhard, J.-G. Zhang, J. Liu, and J. Xiao, *J. Mater. Chem. A*, **1**, 8464 (2013).
67. C. C. Nguyen and S.-W. Song, *Electrochem. Commun.*, **12**, 1593 (2010).
68. G. M. A. Girard, M. Hilder, D. Nucciarone, K. Whitbread, S. Zavorine, M. Moser, M. Forsyth, D. R. MacFarlane, and P. C. Howlett, *J. Phys. Chem. C*, **121**, 21087 (2017).
69. G. M. A. Girard et al., *ACS Appl. Mater. Interfaces*, **10**, 6719 (2018).
70. Y. Domi, H. Usui, K. Yamaguchi, S. Yodoya, and H. Sakaguchi, *ACS Appl. Mater. Interfaces*, **11**, 2950 (2019).
71. M. Dahbi, M. Fukunishi, T. Horiba, N. Yabuuchi, S. Yasuno, and S. Komaba, *J. Power Sources*, **363**, 404 (2017).
72. J. Hwang, K. Matsumoto, Y. Orikasa, M. Katayama, Y. Inada, T. Nohira, and R. Hagiwara, *J. Power Sources*, **377**, 80 (2018).
73. C. Ding, T. Nohira, R. Hagiwara, A. Fukunaga, S. Sakai, and K. Nitta, *Electrochim. Acta*, **176**, 344 (2015).
74. J. Hwang, K. Matsumoto, and R. Hagiwara, *Adv. Sustainable Syst.*, **2**, 1700171 (2018).
75. A. Basile, M. Hilder, F. Makhlooghiazad, C. Pozo-Gonzalo, D. R. MacFarlane, P. C. Howlett, and M. Forsyth, *Adv. Energy Mater.*, **8**, 1870078 (2018).
76. D. Monti, E. Jónsson, M. R. Palacín, and P. Johansson, *J. Power Sources*, **245**, 630 (2014).
77. N. Wongittharom, T.-C. Lee, C.-H. Wang, Y.-C. Wang, and J.-K. Chang, *J. Mater. Chem. A*, **2**, 5655 (2014).
78. C. Ding, T. Nohira, R. Hagiwara, K. Matsumoto, Y. Okamoto, A. Fukunaga, S. Sakai, K. Nitta, and S. Inazawa, *J. Power Sources*, **269**, 124 (2014).
79. C.-Y. Chen, K. Matsumoto, T. Nohira, and R. Hagiwara, *Electrochem. Commun.*, **45**, 63 (2014).
80. K. Matsumoto, Y. Okamoto, T. Nohira, and R. Hagiwara, *J. Phys. Chem. C*, **119**, 7648 (2015).
81. M. Forsyth, H. Yoon, F. Chen, H. Zhu, D. R. MacFarlane, M. Armand, and P. C. Howlett, *J. Phys. Chem. C*, **120**, 4276 (2016).
82. S. Kaushik, J. Hwang, K. Matsumoto, Y. Sato, and R. Hagiwara, *ChemElectroChem*, **5**, 1340 (2018).
83. S. Kaushik, K. Matsumoto, Y. Sato, and R. Hagiwara, *Electrochem. Commun.*, **102**, 46 (2019).
84. P. C. Donohue, W. J. Siemons, and J. L. Gillson, *J. Phys. Chem. Solids*, **29**, 807 (1968).
85. G. J. Fan, F. Q. Guo, Z. Q. Hu, M. X. Quan, and K. Lu, *Phys. Rev. B*, **55**, 11010 (1997).
86. A. W. Weeber and H. Bakker, *Physica B*, **153**, 93 (1988).
87. C. C. Koch, *React. Solids*, **8**, 283 (1990).
88. R. Reinhold, U. Stoeck, H.-J. Grafe, D. Mikhailova, T. Jaumann, S. Oswald, S. Kaskel, and L. Giebeler, *ACS Appl. Mater. Interfaces*, **10**, 7096 (2018).
89. B. H. Park, S. Haghighat-Shishavan, M. Nazarian-Samani, and K.-B. Kim, *J. Power Sources*, **434**, 226759 (2019).
90. B. E. Gurkan, Z. Qiang, Y.-M. Chen, Y. Zhu, and B. D. Vogt, *J. Electrochem. Soc.*, **164**, H5093 (2017).
91. J. Sun, G. Zheng, H.-W. Lee, N. Liu, H. Wang, H. Yao, W. Yang, and Y. Cui, *Nano Lett.*, **14**, 4573 (2014).
92. W.-J. Li, S.-L. Chou, J.-Z. Wang, H.-K. Liu, and S.-X. Dou, *J. Mater. Chem. A*, **4**, 505 (2016).